A mechanism for dynamic lateral polarization in CdZnTe under high flux x-ray irradiation

Derek S. Bale,[a] Stephen A. Soldner, and Csaba Szeles
eV PRODUCTS, Compound Semiconductor Group II-VI Inc., Saxonburg, Pennsylvania 16056, USA

(Received 9 October 2007; accepted 21 January 2008; published online 25 February 2008)

It has been observed that pixillated CdZnTe detectors fabricated from crystals with low hole transport properties ($\mu_h\tau_h < 10^{-5}$ cm^2 V^{-1}) experience a dynamic lateral polarization when exposed to a high flux of x-rays. In this effect, counts are transferred from pixels near the edge of the irradiated region to pixels in the interior. In this letter, we propose a mechanism capable of explaining the observed dynamical effect. The mechanism is based on a transverse electric field that is generated due to space charge that builds within the material. This transverse field, in turn, is responsible for the altered carrier trajectories toward the center of the irradiated region. © *2008 American Institute of Physics*. [DOI: 10.1063/1.2883924]

There is a growing interest in the potentials of pulse-mode CdZnTe detector technology for high-speed multienergy x-ray imaging applications. In particular, medical computer tomography applications represent a large potential market for this technology, but require detectors capable of processing 2×10^8 counts mm^{-2} s^{-1}. Under such intense irradiation, semiconducting radiation detectors with low hole transport properties ($\mu_h\tau_h < 10^{-5}$ cm^2 V^{-1}) suffer a buildup of positive charge that ultimately collapses the electric field and results in catastrophic device failure (i.e., *polarization*).[1–4] Though the charge carrier dynamics that drive a detector to catastrophic failure are predominantly one dimensional,[1] there are, of course, multidimensional dynamics within a polarizing detector that play an important role in x-ray imaging applications. Dynamic lateral polarization in CdZnTe is one such effect that has recently been reported by the authors.[5]

An example of dynamic lateral polarization in a 3 mm thick monolithic CdZnTe detector patterned with a 16×16 array of 0.4×0.4 mm^2 pixels is shown in the plot sequence of Fig. 1. Details of the detector fabrication and experimental test system used are described in Ref. 5. Figures 1(a)–1(d) show the resulting map of pixel counts as the detector is exposed to an increasing flux of x-rays through a 4 mm diameter collimator centered on pixel (9, 6). Figure 1(a) shows the pixel response at low flux with pixels exposed to x rays through the collimator indicated by lighter shades. Figures 1(b) and 1(c) show the pixel response of the same detector at an intermediate flux and high flux, respectively. These plots show that as the flux of x-rays is increased, the counts are symmetrically transferred from pixels near the edge of the irradiated region to the interior. Finally, Fig. 1(d) shows that as the flux is increased further, central pixels ultimately shut off, while a radially symmetric ring of pixels continues to count at a reduced rate.

In this letter, we propose a mechanism capable of explaining the observed dynamic lateral polarization. The mechanism is based on a transverse electric field that is generated due to positive space charge that builds up within the material when subjected to intense irradiation. This transverse field, in turn, is responsible for a lensing of the carrier trajectories toward the center of the irradiated region.

The experimental study reported in Ref. 5 consisted of *n*-type semi-insulating crystals of CdZnTe for which the type was determined by hot-probe measurements,[6] with $\mu_e\tau_e$ products in a range of $(3-10)\times10^{-3}$ cm^2 V^{-1} as measured using a standard Hecht fit.[7] We found and reported that the dynamic lateral polarization effect is exhibited predominantly by detectors with low hole mobility-lifetime products (e.g., for $\mu_h\tau_h < 10^{-5}$ cm^2 V^{-1}). In this work, we consider a detector of thickness L biased at V and exposed to a uniform flux of x-rays Φ_γ passing through a circular collimator of radius R, as shown in Fig. 2(a). Under intense irradiation, low-$\mu_h\tau_h$ detectors will experience strong hole trapping that results in a time-dependent buildup of positive space charge described by[1]

$$\rho(z,t) = \frac{\rho_0}{\lambda}e^{-z/\lambda}(1-e^{-v_{\text{eff}}t/\lambda}), \quad \rho_0 = q\frac{\Phi_\gamma E_\gamma}{v_{\text{eff}}\varepsilon}, \tag{1}$$

where λ is the mean free path in CdZnTe at energy E_γ and ε is the pair creation energy. Once the charge density exceeds a

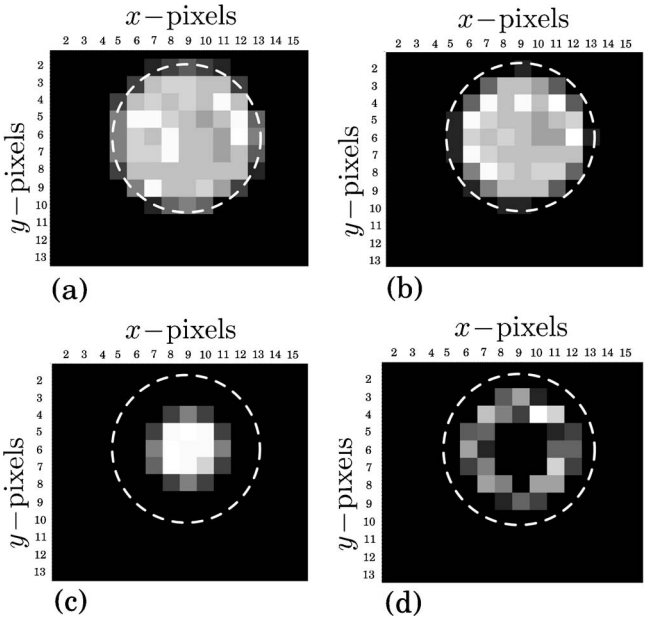

FIG. 1. Counting map for a 3 mm thick, 16×16 pixel CdZnTe monolithic detector array, biased at 900 V and subjected to a (a) low, (b) intermediate, (c) high, and (d) an ultrahigh flux of x-rays through a 4 mm diameter collimator shown as a dashed white line.

[a]Electronic mail: dbale@ii-vi.com.

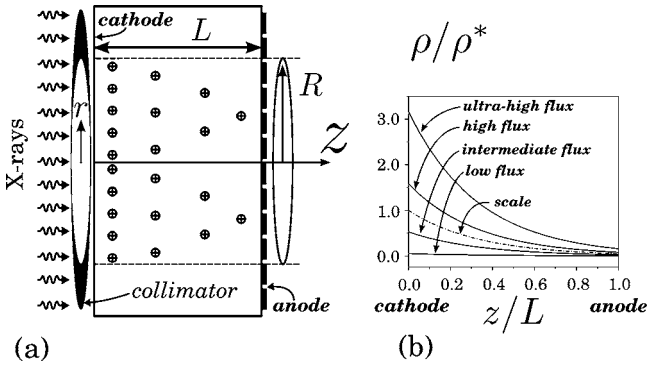

FIG. 2. (a) Detector setup with uniform x-ray irradiation and circular collimator. (b) Depth-wise exponential stationary charge buildup at increasing flux rates.

critical value, namely, $\rho_0 > \rho^* = \epsilon_0 V[1-\exp(-L/\lambda)]^{-1}$, the electric field collapses at a *pinch point* and polarization effects dominate.[1] The characteristic time to polarization, λ/v_{eff}, is controlled by the effective hole velocity $v_{\text{eff}} = [\tau_h/(\tau_h+\tau_D)]\mu_h V/L$, where τ_h and τ_D are the trapping and detrapping times of the dominant hole trap, respectively. A detailed description of v_{eff} and its influence over the dynamics of polarization are given in Ref. 1.

In order to determine the modifications to the electric field induced by the time-asymptotic charge density, we solve the Poisson equation for the electric potential in the irradiated volume of the detector as $t \to \infty$. The cylindrical symmetry of Fig. 2(a) results in the Poisson equation,

$$\left\{\frac{1}{r}\frac{\partial}{\partial r}\left(r\frac{\partial}{\partial r}\right)+\frac{\partial^2}{\partial z^2}\right\}\phi(r,z) = -\frac{\rho_0}{\kappa\epsilon_0}\frac{1}{\lambda}e^{-z/\lambda}, \tag{2a}$$

$$\phi(r,0)=0, \quad \phi(r,L)=V, \quad \phi(R,z)=\frac{V}{L}z, \tag{2b}$$

where κ is the dielectric constant for CdZnTe and ϵ_0 is the permittivity of free space. The boundary condition for $\phi(R,z)$ along the edge of the irradiated region stems from the fact that the potential is linear for regions of the crystal where x-rays are blocked by the collimator. A straightforward application of the separation of variables yields the following solution for the electric potential:

$$\phi = V\frac{z}{L}+\frac{\rho_0}{\kappa\epsilon_0}\left\{\lambda\left[1-e^{-z/\lambda}-\frac{z}{L}(1-e^{-L/\lambda})\right] + \sum_{n=1}^{\infty} a_n I_0(\alpha_n r)\sin(\alpha_n z)\right\}, \tag{3}$$

where $\alpha_n = n\pi/L$ and the coefficients a_n have the form

$$a_n = \frac{2\lambda[1-(-1)^n e^{-L/\lambda}]}{I_0(\alpha_n R)}\left(\frac{n\pi}{(L/\lambda)^2+(n\pi)^2}\right), \tag{4}$$

and I_0 is the zero-order modified Bessel function. This potential is plotted as a surface mesh for a high flux of photons (i.e., $\rho_0 \approx 1.6\rho^*$) in Fig. 3(a). The irradiated region extents through the interval $x \in [-2,2]$ [i.e., $x = r\cos(\theta)$], as indicated by the dashed lines. It is clear from this plot that the linear potential due to the bias voltage has been significantly modified by the presence of the stationary charge within the volume irradiated by the x-rays.

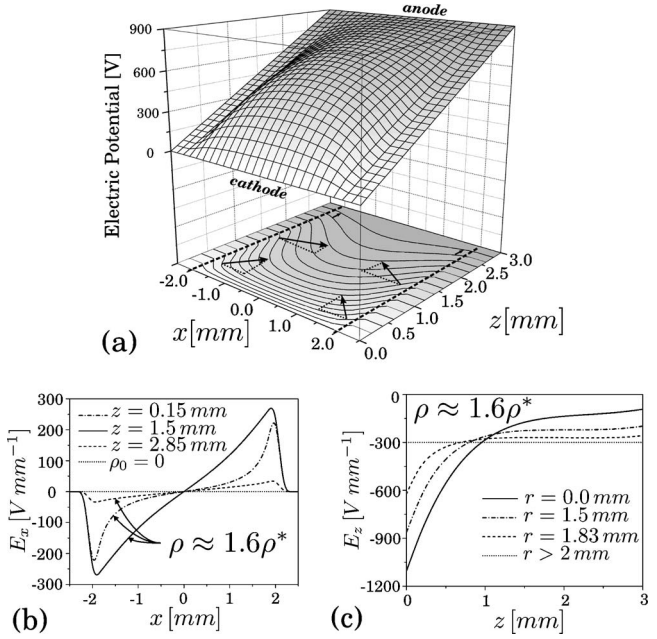

FIG. 3. Solutions for the (a) electric potential $\phi(r,z)$, (b) transverse electric field component E_x, and (c) the depth-wise field component E_z.

The electric field $\vec{E} = -\vec{\nabla}\phi$ that results from the potential in Eq. (3) has a radial component given by

$$E_r = -\frac{\rho_0}{\kappa\epsilon_0}\sum_{n=1}^{\infty} a_n\alpha_n I_1(\alpha_n r)\sin(\alpha_n z). \tag{5a}$$

The corresponding x-component $E_x = \cos(\theta)E_r$ is plotted in Fig. 3(b) for three fixed values of the depth, namely, $z = 0.15$, 1.5, and 2.85 mm. The depth-wise z component of the field has the form

$$E_z = -\frac{V}{L}-\frac{\rho_0}{\kappa\epsilon_0}\left\{\left[e^{-z/\lambda}-\frac{\lambda}{L}(1-e^{-L/\lambda})\right] - \sum_{n=1}^{\infty} a_n\alpha_n I_0(\alpha_n r)\cos(\alpha_n z)\right\}, \tag{5b}$$

and is plotted for fixed $r = 0$, 1.5, and 1.83 mm in Fig. 3(c). Note that since electrons travel against electric field lines, the transverse field component E_x shown in Fig. 3(b) will generate a velocity field with a radial component that points toward the center of the stationary charge distribution, as shown by the arrows in Fig. 3(a).

One of the most interesting features of dynamic lateral polarization is the fact that the lateral constriction of counting pixels is dynamically controlled by the flux of x-rays, as demonstrated in Figs. 1(a)–1(d). This effect is explained in light of the electric field components in Eqs. (5a) and (5b). In Fig. 4, we show the trajectories of electron clouds for a 3 mm detector, biased at 900 V and subjected to the same four increasing fluxes (charge densities) shown in Fig. 2(b). Figure 4(a) shows that at low flux, $\rho_0 < \rho^*$ and the resulting space charge has little affect on the electric field generated by the applied bias. Consequently, the electron clouds generated throughout the detector volume travel in approximately straight lines between the cathode and anode. Assuming uniform charge collection properties, these trajectories will pro-

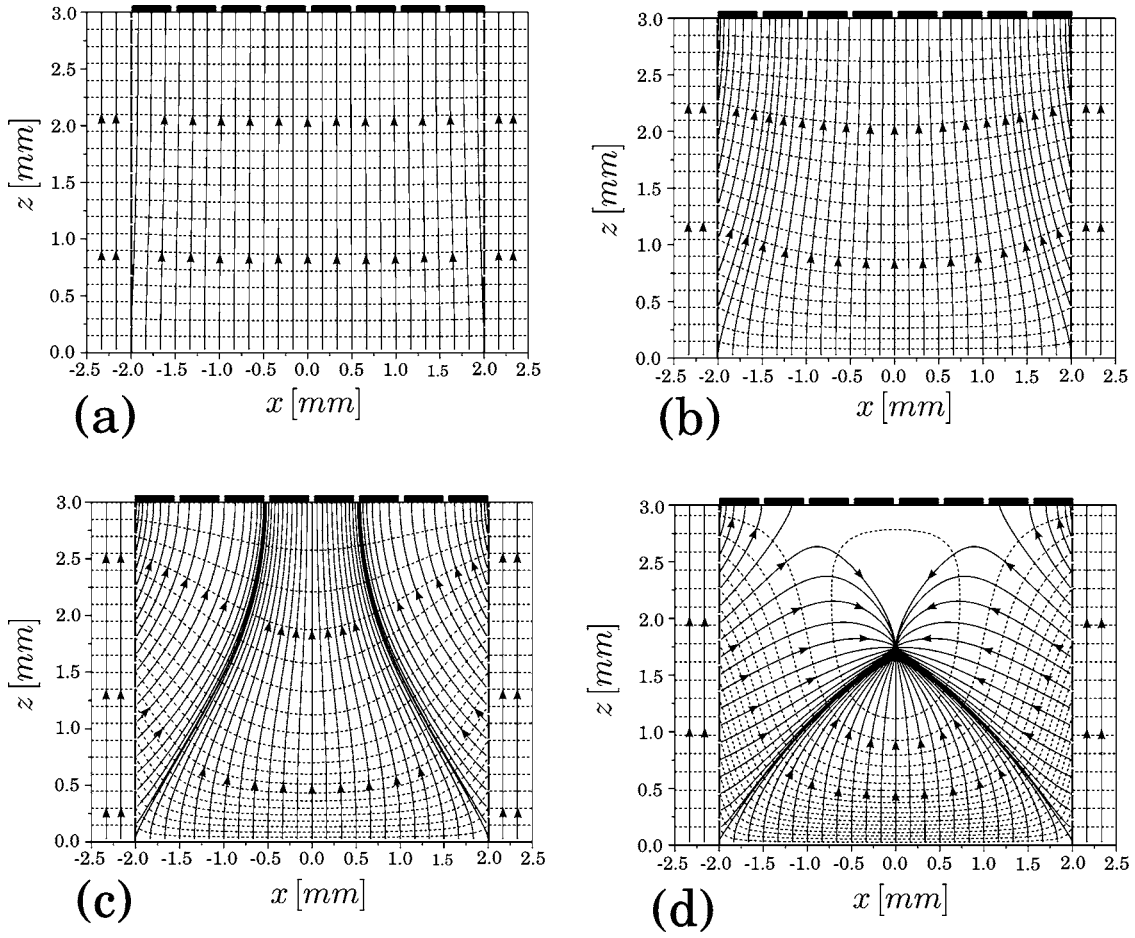

FIG. 4. Electric field lines shown as solid lines with arrows depicting electron trajectories for part of a 3 mm detector, biased at 900 V and subjected to a (a) low, (b) intermediate, (c) high, and (d) an ultrahigh flux of photons through a 4 mm diameter collimator. Equipotential surfaces are shown as dashed curves.

duce uniform counts across illuminated pixels, as shown in the measured low-flux counting map of Fig. 1(a).

In Fig. 4(b), we show the trajectories at an increased flux. At this intermediate flux, there is sufficient stationary charge to create a carrier lensing effect. Note that the electron clouds generated at the cathode and near the edge of the irradiated region are pushed from the edge pixel to the neighboring interior pixel due to the transverse field of Eq. (5a). At this flux, the effect is small so that only the pixels at the edge of the irradiated region lose counts, as shown in the measured counting map of Fig. 1(b).

Increasing the flux further produces electron trajectories, as shown in Fig. 4(c). At this high flux, $\rho_0 > \rho^*$ and the central pixels are collecting the vast majority of the electron clouds generated throughout the detector volume. Though there are electron trajectories that go to the edge pixels, the number of interactions occurring in these modified collection voxels is dramatically reduced because of the fact that a larger fraction of x-rays are absorbed near the cathode plane. The result is a counting map with very bright central pixels surrounded by dark pixels, as shown in Fig. 1(c).

Finally, once the flux is further increased so that the field generates a visible pinch similar to that described in Ref. 1, the electron clouds no longer reach the central pixels, as shown in Fig. 4(d). At this ultrahigh flux, the central pixels shut off completely, and the overall counting rate of all pixels is dramatically reduced. Note, however, that the trajectories in Fig. 4(d) indicate that the pixels near the edge will continue to count even after the central pixels have been polarized. This can be seen in the measured counting map shown in Fig. 1(d), where there is a ring of low-counting pixels near the edge of the collimator that surround central pixels that have completely shut off due to polarization.

In conclusion, we have proposed a mechanism capable of describing the dynamic lateral polarization effect observed in CdZnTe detectors that are fabricated from crystals with low hole transport properties, and subjected to a high flux of x-rays. The mechanism is based on a transverse electric field generated from a positive space charge that develops as a result of excessive hole trapping. We have demonstrated that the electron cloud trajectories derived from the modified electric field are consistent with experimental results.

We acknowledge partial support by the U.S. Army Armament Research, Development, and Engineering Center (ARDEC) under Contract No. DAAE 30-03-C-1171.

[1]D. S. Bale, and Cs. Szeles, Phys. Rev. B **77**, 035205 (2008).
[2]A. Jahnke and R. Matz, Med. Phys. **26**, 38 (1999).
[3]Cs. Szeles, S. A. Soldner, S. Vydrin, J. Graves, and D. S. Bale, IEEE Trans. Nucl. Sci. **54**, 1350 (2007).
[4]D. Vartsky, M. Goldberg, Y. Eisen, Y. Shamai, R. Dukhan, P. Siffert, J. M. Koebel, R. Regal, and J. Gerber, Nucl. Instrum. Methods Phys. Res. A **263**, 457 (1988).
[5]S. A. Soldner, D. S. Bale, and Cs. Szeles, IEEE Trans. Nucl. Sci. **54** (2007).
[6]M. Prokesch and Cs. Szeles, J. Appl. Phys. **100**, 014503 (2006).
[7]K. Hecht, Z. Physik **77**, 235 (1932).